LOADING RESPONSE OF STERN TAB MOTION CONTROLS IN SHALLOW WATER

(DOI No: 10.3940/rina.2016.a2.352)

J Bell, **J Lavroff**, **M R Davis**, University of Tasmania, Australia

SUMMARY

The ride control systems of high-speed vessels frequently use active stern tabs for both motion control and maintenance of correct trim at various speeds and sea conditions. This paper investigates the effect of water depth on the lift force provided by stern mounted trim tabs, of the type fitted to INCAT high speed wave-piercer catamaran vehicle ferries and similar vessels. This investigation was carried out at model scale with the use of a test apparatus in a flume tank in the University of Tasmania hydraulics laboratory. The lift force magnitude and location were measured over a range of tab angles and flow depths. This was used to calculate the lift coefficient of the tab and asses the performance of the tab over the range of flow depths. It was found that the lift force increased and the force location progressed further forward of the hinge as flow depth decreased. The lift curve slope of the stern tab increased by a factor of over 3 relative to the deep water value when the water depth below the hull was approximately equal to the tab chord. The deep water lift curve slope appears to be approached only when the water depth exceeded 4 or more tab chord lengths. The centre of pressure of the lift force was more than two chord lengths ahead of the tab hinge, showing that most of the lift produced by the tab was under the hull rather than on the surface of the tab itself.

NOMENCLATURE

A	Trim tab area (m^2)
α	Trim tab angle below horizontal (rad)
b	Width of elastic link cross section (m)
C_D	Venturi discharge coefficient
C_L	Trim tab lift coefficient
D	Diameter of delivery pipe (m)
d	Venturi throat diameter (m)
E	Young's Modulus of aluminium (N m^{-2})
F	Trim tab lift force (N)
GF	Strain gauge factor
h	Height of elastic link cross section (m)
I	Second moment of area of elastic link (m^4)
l_1	Distance of aft elastic link to tab hinge (m)
l_2	Distance of forward elastic link to tab hinge (m)
M_A	Bending moment about aft elastic link (Nm)
M_F	Bending moment about forward elastic link (Nm)
p	Venturi pressure (N m^{-2})
Q	Volumetric flow rate (m^{3}s^{-1})
R	Strain bridge resistance (Ω)
V	Flow velocity (m s^{-1})
V_{ex}	Strain bridge excitation voltage (V)
V_o	Strain bridge output voltage (V)
x	Distance of lift force effective location to tab hinge (m)
y	Distance from neutral axis of elastic link to strain gauge mounting surface (m)
ε	Strain measured in elastic links
σ	Bending stress in elastic links (N m^{-2})
ρ	Density of water (kg m^{-3})

1. INTRODUCTION

An on-going demand for increasing speed and efficiency of sea transportation has brought about the development of large high speed catamarans, capable of carrying large pay loads at much higher speeds than traditional monohull vessels. To increase competitive advantage ship builders are looking to maximise the payload to ship weight ratio, whilst also increasing stability and operating speeds in more severe sea conditions. The long, slender and widely spaced hulls of catamarans result in vessels which are prone to large heave and pitch motions, and high motion accelerations in heavy seas.

Slamming events are the cause of the most severe forces on catamarans [1], with these events inducing potentially damaging forces and a vibratory response through the ships structure known as whipping [2]. The reduction of ship motions in rough seas is therefore an essential part of the advancement of high speed catamaran design, as these motions are a major contributor to wave and slam loading, in addition to causing passenger discomfort and motion sickness [3]. Research involving both controlled model testing [4, 5, 6], and full scale sea trials [7, 8] has been undertaken in order to quantify and better understand the slamming and whipping response of high speed catamarans. Sea trials have also been undertaken to determine the motion response in a variety of sea conditions [9], and the effectiveness of the fitted ride control systems in damping these motions [10, 11]. Numerical predictions of loads and motions have also been made using the seakeeping code BEAMSEA [12] and finite element analysis.

The INCAT catamaran design utilises a centre bow to limit the occurrence and severity of slam events and to dampen pitching motions, as well as an active ride control system [10, 11]. This system consists of a retractable T-foil mounted at the aft end of the centre-bow and a pair of stern mounted trim tabs. The trim tabs generate a controlled lift force at the ship transom in order to trim the vessel and to reduce rolling motions and, in combination with the forward T-foil, to reduce heave and pitch motions. Sea trials have shown the active ride control system to be effective in reducing the incidence of slam events and damping the motions of the vessel [10]. These sea trials [10] were undertaken with the T-foil both in use, and retracted. The trim tabs however, were always active.

This paper investigates the relationship between flow depth and the lift force produced by testing the trim tabs at model scale at the transom region of an INCAT 112m catamaran model [5]. This will give an indication of the effect shallow was has on the tab lift coefficient and the performance of the ride control system and allow comparison with similar tests conducted in deep flow [13]. A model scale trim tab has been mounted on a test apparatus such that the lift force produced is transferred through two cantilever beams. These beams each have a pair of machined links fitted with strain gauge pairs, allowing the bending moment to be measured at two locations and thus allowing both the applied force and its acting location to be determined.

2. TEST APPARATUS

Testing was carried out in a flume tank in the University of Tasmania Hydraulics Laboratory. The flume has a depth of 400mm and a width of 200mm. The test apparatus is essentially a gate in the flume which causes flow to back up ahead of the gate and accelerate under an extended horizontal base (Figure 1). The base of the apparatus is divided into segments, with the trim tab attached via a hinge at the trailing edge. The base segments are joined by two cantilever beams, through which the resultant tab force is transferred. These beams each have a pair of elastic links machined at the position of the base segment divides. These links have strain gauges fitted to the top and bottom surfaces to form strain gauge pairs, allowing the applied bending moment in the beams to be measured by difference of top and bottom strains. Each pair of strain gauges was operated as a single strain gauge bridge that was calibrated directly for bending moment. This allows the tab lift force magnitude and location to be determined through the calculation from the measured bending moments. The apparatus was designed to test a trim tab at the scale of a 2.5m long hydroelastic segmented model of the 112m INCAT catamaran [5].

Equations (1) and (2) are the equations for the measured forward and aft bending moments, which can be solved to determine the magnitude of the applied force F, and its effective point of location relative to the tab hinge, x.

$$M_F = F(x + l_1 + l_2) \quad (1)$$

$$M_A = F(x + l_1) \quad (2)$$

where l_1 and l_2 are the distances from the forward and aft elastic links to the tab hinge.

Mounting clamps secured the front and rear of the forward section to rails above the flume walls, and were adjustable to allow varying flow depths to be used. The apparatus base, beams and mounting clamps were constructed from aluminium. The apparatus also included Perspex side walls to prevent flooding on the top side of the base during testing. The 195mm overall width provided a small sealable clearance between the apparatus and the flume walls. This allowed the use of the forward section as a gate in the flume to accelerate flow under the base, while allowing the aft segments to have freedom of movement. All gaps between the segments, both on the base and Perspex sidewalls, were sealed with latex and tape to provide a flexible but watertight seal. The apparatus design is shown in Figure 2, while the measured key dimensions as used in calculations are given in Table 1.

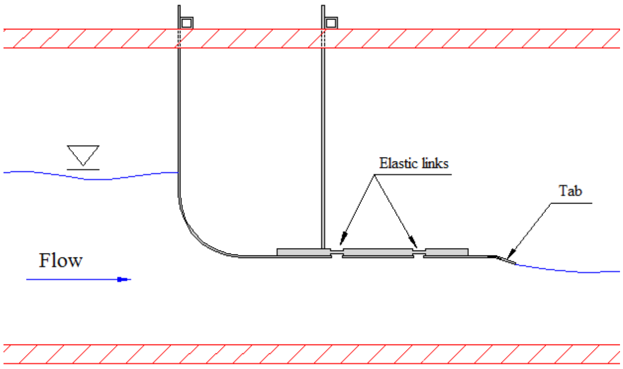

Figure 1: Schematic of experimental setup.

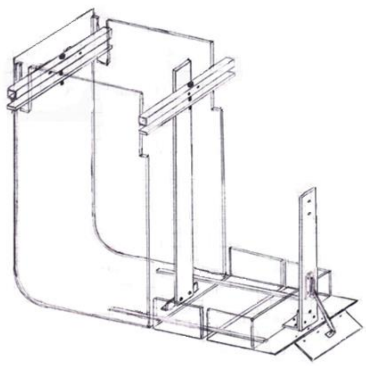

Figure 2: Sketch of apparatus design.

Table 1: Apparatus key dimensions

Elastic Links			
	b (m)	h (m)	I_x (m^4)
Forward Left	0.00801	0.0048	7.382E-11
Forward Right	0.00803	0.00481	7.447E-11
Aft Left	0.0081	0.00342	2.700E-11
Aft Right	0.00792	0.00342	2.640E-11
Trim Tab Dimensions			
Effective Length (hinge centre to trailing edge) (m)	0.037		
Tab Width (m)	0.130		
Lever arms			
l_1 (m)	0.12		
l_2 (m)	0.245		

The two machined elastic links in each of the longitudinal beams were sized such that a vertical force applied at the tab hinge would induce a similar strain of predicted magnitude at both the forward and aft link locations. The strain gauges mounted on the top and bottom surfaces of these links formed strain gauge pairs and were wired in half bridge configuration, with the bridge output voltages being amplified and recorded to a PC with the use of LABVIEW. For each gauge pair the output voltage, V_o, was produced from the strain gauge resistances R_3 and R_4, bridge resistances R_1 and R_2 and the bridge excitation voltage V_{ex} as given in Equation 3. Equation 4 gives the measured strain ε for each gauge pair as calculated from the output voltage, where GF is the strain gauge factor for the specific strain gauges used:

$$V_0 = \left(\frac{R_4}{R_3+R_4} - \frac{R_2}{R_1+R_2}\right) V_{ex} \tag{3}$$

$$\varepsilon = \frac{-2V_o}{V_{ex}GF} \tag{4}$$

Simple beam theory then can be used to calculate the bending moment for each link M at the strain gauge locations from the measured strain in terms of the surface stress σ by re-arranging Equation (5) and substituting the required values to give Equations (6) and then (7). The value y is the distance from the centroid to the link surface, and the second moment of area I.

$$\sigma = \frac{My}{I} \tag{5}$$

$$bh^2 = \frac{6M}{E\varepsilon} \tag{6}$$

$$M = \frac{bh^2 E\varepsilon}{6} \tag{7}$$

The total bending moments M_F and M_A at the forward and aft connection sections are then the sum of the moments from the pair of links at each section. Equations (8) and (9) can be deduced from Equations (1) and (2), which then make use of the measured bending moments to give the measured force magnitude and location:

$$F = \frac{(M_F - M_A)}{(l_2)} \tag{8}$$

$$x = \frac{M_A}{F} - l_1 \tag{9}$$

3. CALIBRATION

Calibration of the measured strain readings was performed by measuring the output for known loads. The loads were applied at the point of the tab hinge while the apparatus was positioned upside down with the base horizontal, thus achieving the same loading direction as applied during testing. The loads were increased incrementally to give a trend of measured force from the strain readings against the known applied force from the load. The latex seals were fitted to the apparatus prior to calibration in such a way that they were not under tension during loading. This was done to prevent tension in the latex influencing results during testing.

The output voltage readings from the strain gauge pairs were used to calculate the strain and applied bending moments at the elastic link locations as described in section 2. This allowed an applied force value to be calculated at the forward and aft link locations using the measured lever arm distances and the calculated bending moment. A plot of calculated force values at both link locations against the actual applied force is shown in Figure 3. This shows that the measured force deviates from the actual applied force by a small but constant factor over the loading range. This calibration factor could be due to and accounts for discrepancies between the actual and measured link dimensions, bridge setup errors and differences between the assumed and actual Young's Modulus of the aluminium.

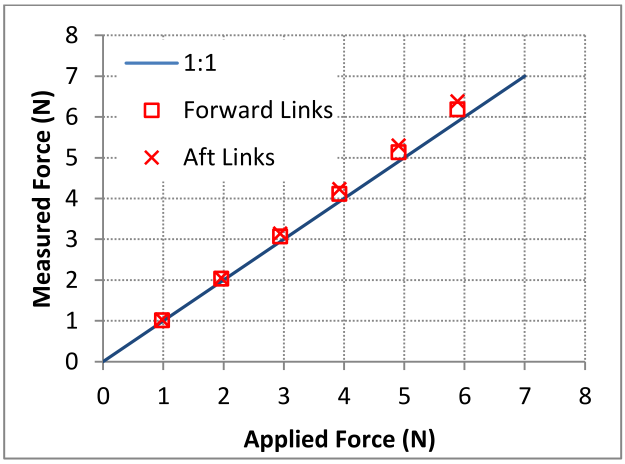

Figure 3: Apparatus calibration.

4. TESTING

A venturi nozzle and electronic pressure transducer were used to measure the flow rate delivered by the pump, with a maximum flow rate of 0.0215 m^3/s available. Flume tank flow depths of 40, 60 and 77mm were used during testing. These depths were somewhat dictated by the available flow in the flume and the desired flow velocities. Trim tab angles from 0^o (horizontal) to 20^o were tested at increments of 5^o.

The output strain data was displayed graphically on a PC as output voltage against time for each strain gauge pair, with the data being saved in Microsoft Excel. Readings averaged over a constant input time period were then used to calculate the bending moment at each link location, and then the magnitude and location of the lift force provided by the tab.

The sampling rate in the LABVIEW data acquisition program was set to 10 Hz and the output voltage signal from each strain gauge pair was zeroed with the apparatus in position in the dry flume. Measurements were taken at each flow depth setting for a range of flow velocities and tab angles. Maximum flow velocities at each flow depth were restricted by the maximum pump flow, while the minimum was restricted by the need to prevent flooding of the trim tab by a hydraulic jump downstream of the model wave in the flume, while still having flow contact the base of the apparatus.

Figure 4 shows the test apparatus in the flume during testing. The stern tab during test conditions and the resulting effect on the flow is shown in Figure 5.

Figure 4: Experimental apparatus during testing.

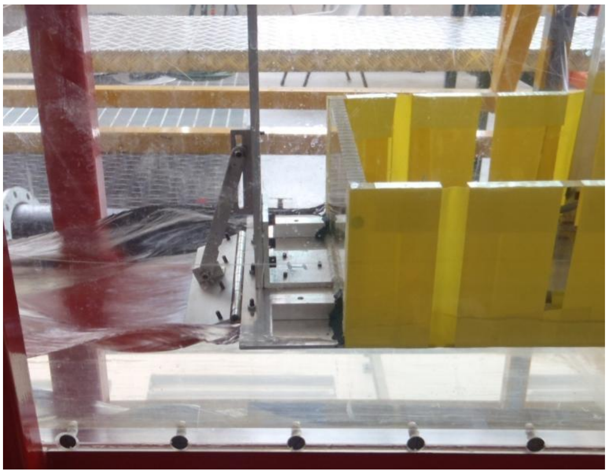

Figure 5: Detail of tab during testing.

5. DATA PROCESSING AND ANALYSIS

The measured resultant force magnitude and location produced by the flow under the trim tab was calculated by processing the raw output data in Microsoft Excel. This included measurements taken without the trim tab in contact with the flow, so as to provide a reference for the flow acting on the base of the apparatus without influence from the tab. The decrease in flow area with increasing tab angle and the resulting acceleration of the flow was also considered in calculating the flow velocity.

The velocity of the flow acting on the tab was calculated using the flow cross sectional area at the tab and the volumetric flow rate, Q, calculated from the venturi reading as per Equation 10:

$$Q = C_D\left(\frac{\pi d^2}{4}\right)\sqrt{\frac{2\Delta p}{\rho\left(1-\left(\frac{d}{D}\right)^2\right)}} \tag{10}$$

The measured force magnitude is shown as a function of flow velocity in Figure 6, with the varying flow depths shown by dissimilar data point markers. Trim tab angles are included next to the corresponding data set. The results as expected show the lift force increasing with flow velocity over the tested range of approximately 1.1 to 2.5 m/s. However for each reduction in flow depth, there is a step up in measured force for a given flow velocity. There is a relatively constant increase in force with increase in tab angle up to 15°, but the increase is smaller from 15° to 20°.

The gradient of the increase in lift force is also seen to reduce for flow velocities beyond 2 m/s despite the expected quadratic trend. While these results suggest that the lift coefficient of the tab drops at higher tab angles and higher flow velocities, it must be noted that the increase in lift force under these conditions increases the upward deflection in the apparatus base, somewhat reducing the effective tab angle relative to the flume. However, allowing for the stiffening effect of the base plates attached to the support beams, this is estimated to be less than 0.5 deg at the maximum lift of approximately 25N. The influence of blockage due to the flume side walls is also expected to be more significant as tab angle and flow velocity increase.

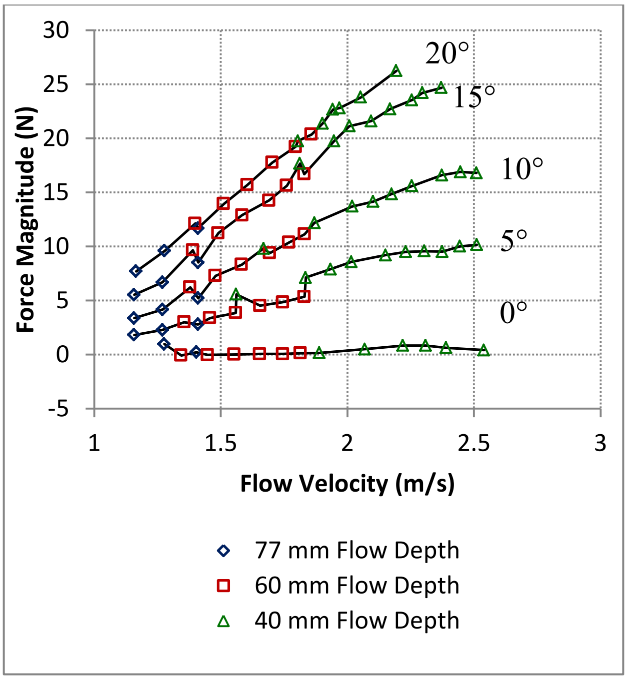

Figure 6: Magnitude of tab lift force versus flow velocity, grouped by varying depth for stern tab angles 0, 5, 10, 15, and 20 degrees.

The lift force magnitude and flow velocity can be used to calculate a measured lift coefficient value for the tab, as shown by equation 11.

$$C_L = \frac{F}{\left(\frac{1}{2}\rho V^2 A\right)} \tag{11}$$

The lift coefficient gives a more useful indication of the measured tab performance in dimensionless form. Figure 7 shows the lift coefficient against flow velocity and Figure 8 shows the lift coefficient against tab angle. Figure 7 shows a relatively small step increase in lift coefficient with each reduction in flow depth, with the lift coefficient being relatively constant across all velocities for the two deeper flows at each tab angle. The reduction in measured performance at higher flow velocities causes the results to trend downwards for the 40mm depth. Figure 8 shows the lift coefficient increase seen between the 77mm and 60mm flow depths. However the apparent reduction in tab performance at higher flow velocities causes the results from the 40mm depth to be spread and any step increase in lift coefficient is less defined.

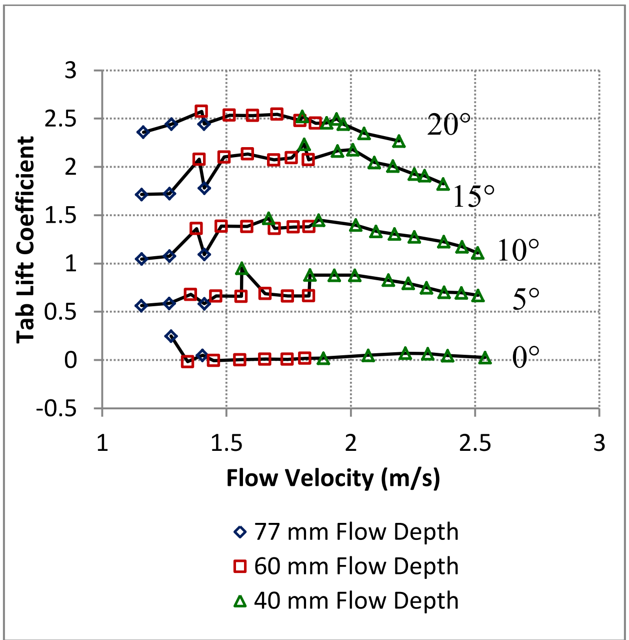

Figure 7: Tab lift coefficient versus flow velocity, grouped in flow depths. Tab angles 0, 5, 10, 15 and 20 degrees.

Figure 9 shows the variation of the lift curve slope $dC_L/d\alpha$ with the ratio of flow depth to tab length, with the two deeper flows giving consistent values, while the minimum flow depth shows a wider range of values as speed and tab deflection vary. The average $dC_L/d\alpha$ value for each flow depth is given in table 2.

These figures show that in general, a decrease in flow depth brings about an increase in lift coefficient. This is most pronounced for change in depth from 77mm to 60mm at tab angles of 10 and 15 degrees. The further reduction to a 40mm flow height shows less of an increase in lift coefficient, with values tapering downwards as the flow velocity increases. This is consistent with the data seen in Figure 6 and suggests that the increased apparatus deflection (expected to be small as discussed above) and/or an increase in blockage effects may be affecting the results at the shallowest depth tested.

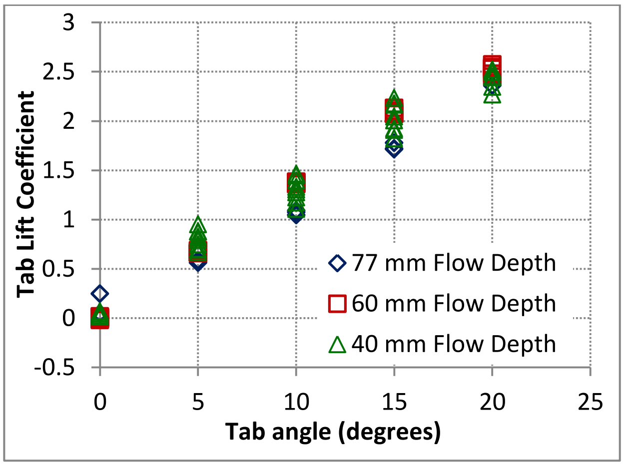

Figure 8: Tab lift coefficient versus tab angle, grouped in flow depths (all speeds).

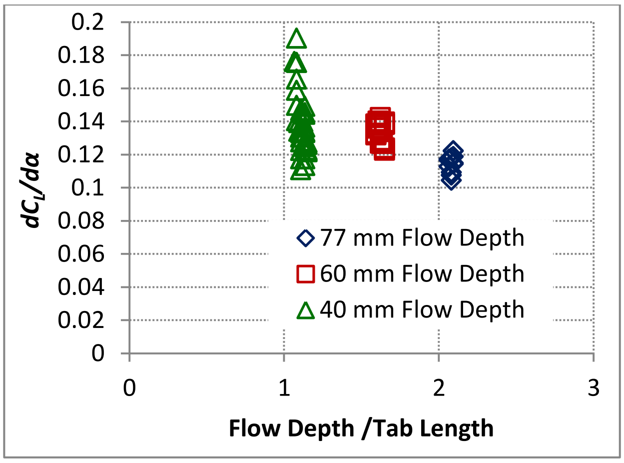

Figure 9: Change in lift coefficient with change in tab angle plotted against flow depth relative to tab length (all flow speeds and all tab angles).

Table 2: Average $dC_L/d\alpha$ at each flow depth.

Approximate Flow Depth	**Average $dC_L/d\alpha$**
77 mm	0.115
60 mm	0.134
40 mm	0.139

The effective location of the lift force generated by the trim tab is able to be calculated from the bending moment values for the two link locations, allowing a point of action to be determined. This effective force location, relative to the tab hinge, is shown in Figure 10. It can be seen that the force location was relatively constant for the test cases at the two deeper flows. The distance of the force forward of the tab is seen to step down, then further reduce with an increase in flow velocity at the minimum flow depth, showing a similar trend to the reduction in force magnitude. The average distance of the force forward of the tab is relatively large compared to the overall tab length, with the two largest flow depths giving an average distance of approximately 65 mm forward of the tab.

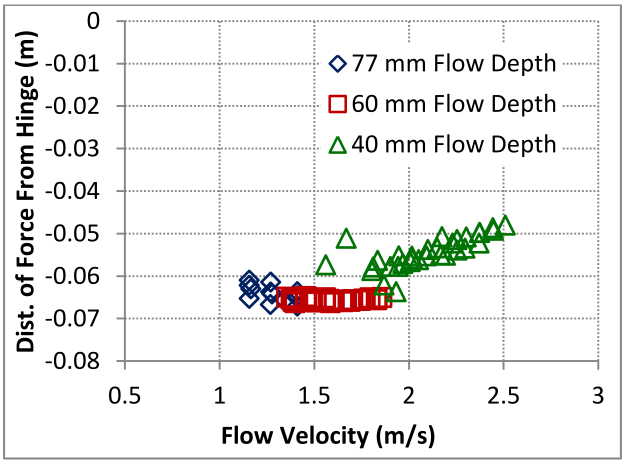

Figure 10: Effective lift force location relative to hinge, grouped in flow depths (negative x indicates a location forward of the tab hinge, tab chord =0.037m).

In addition to the effect of the flow depth on the pressure distribution on the underside of the modelled hull, it is possible that the width of the flume may also have some effect on the measured forces. The test flume is almost 200mm wide and in these tests the trim tab spans 65% of the flume width.

6. COMPARISON WITH DEEP WATER

The same test apparatus has been modelled with CFD and used to conduct deep flow analysis [14]. The CFD analysis and deep flow testing returned very similar results but were significantly different to those obtained from the present shallow water tests.

The deep flow testing in [13] returned a $dC_L/d\alpha$ value of 0.044, compared to those given in Table 2 of this paper. Figure 11 illustrates this comparison. This comparison is consistent with the increase in lift force with decrease in flow depth seen during the testing discussed in this paper, and indicates that even at the deepest (77 mm) flow tested, the depth has had a large effect on results. Figure 11 indicates that whilst the effect of the water bottom decreases as depth increase, a substantially larger depth than that tested here would be needed to achieve effectively infinite depth conditions. From the trend shown in Figure 11 it appears that infinite depth conditions will only be reached when the water depth below the hull exceeds approximately 4 tab chord lengths. Whilst Figure 11 shows the lift curve slope as a function of depth/chord ratio, it should be noted that the pressure distribution extends significantly upstream of the hinge, as evidenced by the forward location of the resultant lift force more than two chord lengths ahead of the hinge line. Thus normalisation of the depth by the tab chord yields much higher ratios than that which would be more directly representative of the interaction of the water bottom with the flow and pressure fields beneath the hull and tab. Clearly the lift force would still be considerably affected by the flow depth for a range of deeper values than tested here.

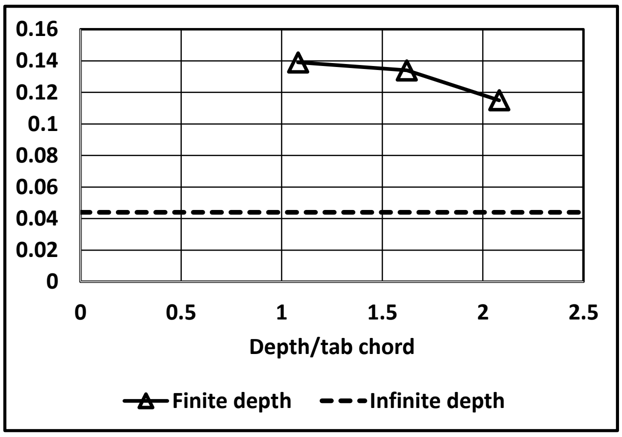

Figure 11: Variation of $dC_L/d\alpha$ with water depth showing finite depth shallow water data (Table 2) for comparison to infinite depth results presented in [14].

These deep flow tests also found the force to act at distance approximately equal to or greater than the tab cord length forward of the hinge, which is considerably closer to the hinge than in the shallow water tests presented here. This result is consistent with the force data in suggesting that flow blockage has a significant effect as shallow flow depth.

7. CONCLUSIONS

The results obtained from the test data show that a change in flow depth causes a substantial increase in the magnitude of the lift force produced by the trim tab. A decrease in flow depth was shown to bring about an increase in lift force for any given flow velocity and tab deflection. This is generally consistent with added restriction of flow in shallow water causing an increase of velocity beneath the tab and thus higher pressures ahead of the tab trailing edge.

The limitations of the test procedure inevitably introduce some uncertainties into the specific values obtained here. However the overall trend in the results appears clear and the results demonstrate an important consideration for the performance of ride control systems. The effect of shallow water on the performance of the trim tab is relevant to the full scale vessel, but is likely to be of much larger consequence to model testing, where setups are often restricted in test tank depth. Further controlled testing would be required to determine the tab performance as water depth increases more closely towards the deep water condition. The results of such tests could then be used to determine the minimum working depth for unaffected testing, and the degree of influence shallow water will have on a ships ride control performance. However, the indications of the present work is that depth effects will only be absent when the depth exceed approximately 4 tab chord lengths.

8. REFERENCES

1. LAVROFF, J., DAVIS, M. R., HOLLOWAY, D. S., THOMAS, G., Determination of Wave Slamming Loads on High-Speed Catamarans by Hydroelastic Segmented Model Experiments, *International Journal of Maritime Engineering*, *Volume 153 (A3), pp 185-197,* 2011.
2. THOMAS, G., DAVIS, M. R., HOLLOWAY, D. S. ROBERTS, T. J., The Whipping Vibration of Large High-Speed Catamarans, *Transactions of the Royal Institution of Naval Architects, Volume 145 (A4), pp 13-29,* 2003.
3. DAVIS, M. R., HOLLOWAY, D. S., Motion and Passenger Discomfort on High Speed Catamarans in Oblique Seas, *International Shipbuilding Progress*, *Volume 50, (4)pp 333-370,* 2003.
4. LAVROFF, J., DAVIS, M. R., HOLLOWAY, D. S., THOMAS, G., The Vibratory Response of High Speed Catamarans to Slamming Investigated by Hydroelastic Segmented Model Experiments,*Transactions of the Royal Institution of Naval Architects, Volume 151 pp 1–12,* 2010.
5. LAVROFF, J., The Slamming and Whipping Vibratory Response of a Hydroelastic Segmented Catamaran Model, *PhD Thesis, University of Tasmania,* 2009.
6. THOMAS, G., WINKLER, S., DAVIS, M. R., HOLLOWAY, D. S., MATSUBARA, S., LAVROFF, J., FRENCH, B., Slam Events of High-Speed Catamarans in Irregular Waves, *Journal of Marine Science and Technology, Volume 16*, *pp 8-21,* 2010.
7. THOMAS, G., DAVIS, M. R., HOLLOWAY, D. S., WATSON, N. L., ROBERTS, T. J., Slamming Response of a Large High-Speed Wave-Piercer Catamaran, *Marine Technology, Volume 40 (2), pp 126–140,* 2003.
8. THOMAS, G., DAVIS, M. R., ROBERTS, T. J., Transient Dynamic Slam Response of Large High-Speed Catamarans, *7th International Conference on Fast Sea Transportation, FAST '03,* 2003.
9. DAVIS, M. R., WATSON, N. L., HOLLOWAY, D. S., Measurement of Response Amplitude Operators for an 86 m High-Speed Catamaran,*Journal of Ship Research, Volume 49, pp 121-143,* 2005.
10. JACOBI, G., High-speed Catamaran Motion Response and Slamming Behaviour During Full Scale Trials, *Diploma of Engineering (Naval Architecture) Masters Thesis, University Rostock,* 2011.
11. SHAHRAKI, J. R., DAVIS, M. R., SHABANI, B., ALAVIMEHR, J., THOMAS, G. A., LAVROFF, J., AMIN, W. A. I., Mitigation of Slamming of Large Wave-Piercing Catamarans, *30th Symposium on Naval Hydrodynamics, Hobart, Tasmania, Australia, pp on CD,* 2014.
12. HOLLOWAY, D. S., DAVIS, M. R., Ship Motion Using a High Froude Number Time Domain Strip Theory, *Journal of Ship Research, Volume 50, pp 15-30,* 2006.
13. BELL, J., ARNOLD, T., LAVROFF, J., DAVIS, M. R., Measured Loading Response of Model Motion Control Stern Tabs, *International Journal of Maritime Engineering, Volume 155 (A1), pp 1-7,* 2013.
14. ARNOLD, T., LAVROFF, J., DAVIS, M. R., Pressure Distribution due to Stern Tab Deflection at Model Scale, *International Journal of Maritime Engineering, Volume 157 (A1), pp 31-40,* 2015.